Reversible, irreversible, and mixed regimes for periodically driven disks in random obstacle arrays

D. Minogue,[1] M. R. Eskildsen,[1] C. Reichhardt,[2] and C. J. O. Reichhardt[2]
[1]*Department of Physics, University of Notre Dame, Notre Dame, Indiana 46656, USA*
[2]*Theoretical Division and Center for Nonlinear Studies, Los Alamos National Laboratory, Los Alamos, New Mexico 87545, USA*

(Received 31 January 2024; accepted 27 March 2024; published 19 April 2024)

We examine an assembly of repulsive disks interacting with a random obstacle array under a periodic drive and find a transition from reversible to irreversible dynamics as a function of drive amplitude or disk density. At low densities and drives, the system rapidly forms a reversible state where the disks return to their exact positions at the end of each cycle. In contrast, at high amplitudes or high densities, the system enters an irreversible state where the disks exhibit normal diffusion. Between these two regimes, there can be an intermediate irreversible state where most of the system is reversible, but localized irreversible regions are present that are prevented from spreading through the system due to a screening effect from the obstacles. We also find states that we term "combinatorial reversible states" in which the disks return to their original positions after multiple driving cycles. In these states, individual disks exchange positions but form the same configurations during the subcycles of the larger reversible cycle.

DOI: 10.1103/PhysRevE.109.044905

I. INTRODUCTION

There are a variety of systems that can be modeled as a collection of particles driven over a disordered landscape, such as vortices in type-II superconductors [1,2], colloidal particles [3], magnetic skyrmions [4,5], emulsions [6], active matter [7,8], and granular matter [9]. The quenched disorder can be in the form of pinning sites that act as local traps, such as those found in superconducting vortex systems, or of obstacles, such as those found in soft-matter systems. Other examples of this type of dynamics include particulate matter flowing through disordered media or bottlenecks, where clogging phenomena can occur [10–13]. In systems with pinning or obstacles, the drive responsible for producing flow is generally applied only along one direction; however, in some situations the drive is oscillating, and in this case, it is possible for reversible motion to appear in which the particles return to the same positions at the end of each drive cycle or after a fixed number of cycles [14].

Reversible to irreversible (R-IR) transitions in the absence of pinning or obstacles have been studied in a variety of systems. One of the simplest of these systems is dilute suspensions of colloids under a periodic shear, where it was shown that for a fixed colloid density, there is a critical shear amplitude below which the system organizes to a reversible state, while at high amplitude, the system remains in a chaotic state where the particles exhibit diffusive behavior [15,16]. If the drive amplitude is fixed, there is also a critical density below which the system forms a reversible state. Similar R-IR transitions have been studied in other periodically sheared dilute systems where, in some cases, the reversible states were found to exhibit hyperuniformity [17–21]. For the dilute system, the reversible states are usually those in which collisions between the particles no longer occur, and such states have been shown to be capable of encoding memories of the number of cycles through which the system passed on the way to the reversible state [22,23]. R-IR transitions have also been studied in dense systems where the particles are in continuous contact, such as granular matter [24,25] or amorphous solids. In this case, the reversible state of the system is marked by reversible plastic events [26–31]. Dense systems can also show reversibility after multiple cycles due to the appearance of multiple plastic events that interact by long-range strain fields [26,32–34].

R-IR transitions can also occur in systems that exhibit pinning or clogging dynamics, where the cyclically driven particles interact with quenched disorder [2]. Such systems include vortices in type-II superconductors [35–39], magnetic skyrmions [40,41], and colloidal particles [13]. One difference between systems with and without quenched disorder is that when quenched disorder is present, R-IR transitions can be induced with a uniformly applied drive rather than through shearing; however, under uniform driving in the absence of quenched disorder or thermal fluctuations, only reversible states form. Systems with quenched disorder can behave elastically, where particles maintain the same nearest neighbors over time, or plastically, where deformations cause particles to exchange neighbors or lead to the coexistence of flowing and pinned states [2].

In cyclically driven superconducting vortex systems, plastic deformations were shown to result in the particles undergoing chaotic motion, while when the drive or pinning is weak, the system can form reversible orbits [35–39]. In superconducting vortex and magnetic skyrmion systems, the quenched disorder takes the form of randomly located trapping sites; however, there have also been studies of R-IR transitions in cyclically driven disk systems interacting with a periodic array of obstacles [42]. For the latter case, when the driving is applied along a symmetry direction of the obstacle array, the system forms reversible and spatially ordered states; however, for drives applied along angles that are incommensurate with the array symmetry, the system forms an irreversible

 ©2024 American Physical Society

state even at low drives. Stoop *et al.* [13] also considered disks moving over a random array of obstacles under a forward and backward pulse drive, and found that the system can form a partially clogged state with different configurations during different portions of the drive. This work suggests that R-IR transitions could also be possible in disordered obstacle arrays.

Here, we consider a two-dimensional assembly of disks cyclically driven over a random array of obstacles. We find that for high drive amplitudes or high disk densities, the system forms irreversible states with diffusive behavior, while for lower drives and densities, reversible states occur that return to the original configuration after one or more drive cycle. We map out the onset of the R-IR transition as a function of disk density and drive amplitude. In some cases, the reversible states consist of clogged regions that coexist with regions of moving disks, while the irreversible states can also form heterogeneous configurations that change from one cycle to the next. Near the R-IR boundary, we find what we call intermediate irreversible states where most of the system is reversible, but there are localized irreversible regions that are screened from rapidly spreading through the system by a trapping effect of the obstacles. This leads to extended times during which the system behaves subdiffusively. The localized chaotic regions slowly move through the system after many cycles. We also find states that do not have long-time diffusion but contain small chaotic regions that remain localized. We observe a number of states that are reversible after multiple cycles, and term these combinatorial reversible states. They are associated with groups of disks that exchange positions such that after N cycles, the macroscopic disk configuration is the same but the microscopic positions of the disks differs. The system returns to the exact same configuration of the original disks after multiples of the N cycles. These combinatorial multicycle states are distinct from the multiple-cycle states found in amorphous solids, which occur due to longer-range elastic interactions. In our disk system, they occur due to purely local contact interactions.

II. SIMULATION

We examine a two-dimensional system of size $L \times L$ containing N_d mobile disks of radius $r_d = 0.5$ and $N_{\rm obs}$ obstacles of radius $r_{\rm obs} = 1.025$. The sample has periodic boundary conditions in the x and y directions. The density ρ is defined to be the area covered by the obstacles and mobile disks, $\rho = N_{\rm obs}\pi r_{\rm obs}^2/L^2 + N_d\pi r_d^2/L^2$, where we fix $L = 36$. We also fix the number of obstacles to $N_{\rm obs} = 80$, which corresponds to an obstacle density of 0.204. We vary the number of mobile disks N_d from 20 to 650 in increments of 50, giving a total disk density that varies from $\rho = 0.216$ to $\rho = 0.598$ in increments of 0.03. The density of mobile disks ranges from a few percent to about twice the obstacle density, so we span the very dilute mobile disk limit to the interacting limit.

The dynamics of the mobile disks is obtained from the following overdamped equation of motion:

$$\alpha_d \mathbf{v}_i = \mathbf{F}_i^{\rm dd} + \mathbf{F}_i^{\rm obs} + \mathbf{F}^{\rm D}. \tag{1}$$

Here, α_d is the damping constant, which we set to unity. The disk velocity is $\mathbf{v}_i = d\mathbf{r}_i/dt$, where $\mathbf{r}_i$ is the location of disk i. The disk-disk interaction force $\mathbf{F}_i^{\rm dd} = \sum_{j\neq i}^{N_d} k(D - r_{ij})\Theta(D - r_{ij})\hat{\mathbf{r}}_{ij}$ is represented by a short-range harmonic repulsive potential, where $D = 2r_d$, k is the spring constant, $r_{ij} = |\mathbf{r}_i - \mathbf{r}_j|$, and $\hat{\mathbf{r}}_{ij} = (\mathbf{r}_i - \mathbf{r}_j)/r_{ij}$. The disk-obstacle interaction term $\mathbf{F}_i^{\rm obs}$ has the same form as $\mathbf{F}^{\rm dd}$ but with $D = r_d + r_{\rm obs}$, so that the obstacles are represented as randomly located nonoverlapping immobile disks of radius $r_{\rm obs}$. Our disks have no rotational degrees of freedom. Rotation can be relevant in physical systems of grains and colloids, and it would be interesting for a future study to see if additional rotational degrees of freedom affect the reversible to irreversible transitions. This could be particularly relevant for particles that are not perfectly circular.

The driving force $\mathbf{F}^{\rm D} = \pm A\hat{\mathbf{x}}$ is a zero-centered square wave of amplitude A and period $T = 4 \times 10^5$ simulation time steps, where the positive sign is used during the first half of each period and the negative sign is used during the second half period. As a measurement of time we use the quantity N_c, which is the total number of driving cycles that have elapsed since the beginning of the simulation. We hold T fixed throughout this work and vary A over the range $A = 0.01$ to $A = 0.0425$ in intervals of 0.0025. To initialize the system, we first place the obstacles in randomly chosen nonoverlapping positions, and then add mobile disks in randomly chosen positions that do not overlap with obstacles or other mobile disks. Five different disorder realizations are performed for each set of parameters.

To quantify the number of disks that return to their original positions after n driving cycles, we measure the difference between the disk positions at a reference time t_0 and a time $t_0 + nT$ that is exactly n driving cycles later: $R(n) = \sum_i^{N_d}[\mathbf{r}_i(t_0 + nT) - \mathbf{r}_i(t_0)]$. When $R(n) = 0$, the motion is reversible after n driving cycles. If $R(1) = 0$, then the motion is reversible after only a single driving cycle. A disk is defined to have returned to its original position if the disk center is within 0.1% of its original position. The total distance traveled by the disks after N_c cycles have elapsed from a reference time t_0 is given by $d(N_c) = \sum_i^{N_d} |\mathbf{r}_i(t_0 + N_c) - \mathbf{r}_i(t_0)|$. In an irreversible state, $d(N_c)$ will grow continuously as a function of N_c. Since N_c is proportional to time, we also characterize irreversibility by fitting $d \propto N_c^{\alpha}$, where $\alpha = 0$ for reversible motion, $\alpha = 1.0$ for Brownian diffusion, and $0 < \alpha < 1$ for subdiffusion.

III. RESULTS

In Fig. 1(a) we show a snapshot of the obstacle and disk positions in the completely reversible state at $A = 0.02$ and $\rho = 0.368$. The snapshot is taken at the end of the drive cycle when the drive is about to switch from the $-x$ direction back to the $+x$ direction. We find that a reversible state can appear even when some disks come into contact with other disks, in contrast with the sheared dilute disk systems, where the reversible states involve no disk collisions. Some of the disks become clogged in bottleneck configurations during portions of the drive cycle, and these stuck regions coexist with other regions where the disks continue to move throughout the cycle. When the drive direction switches, the bottleneck regions are released and become mobile again, but new bottlenecks can form in different locations for the reversed driving

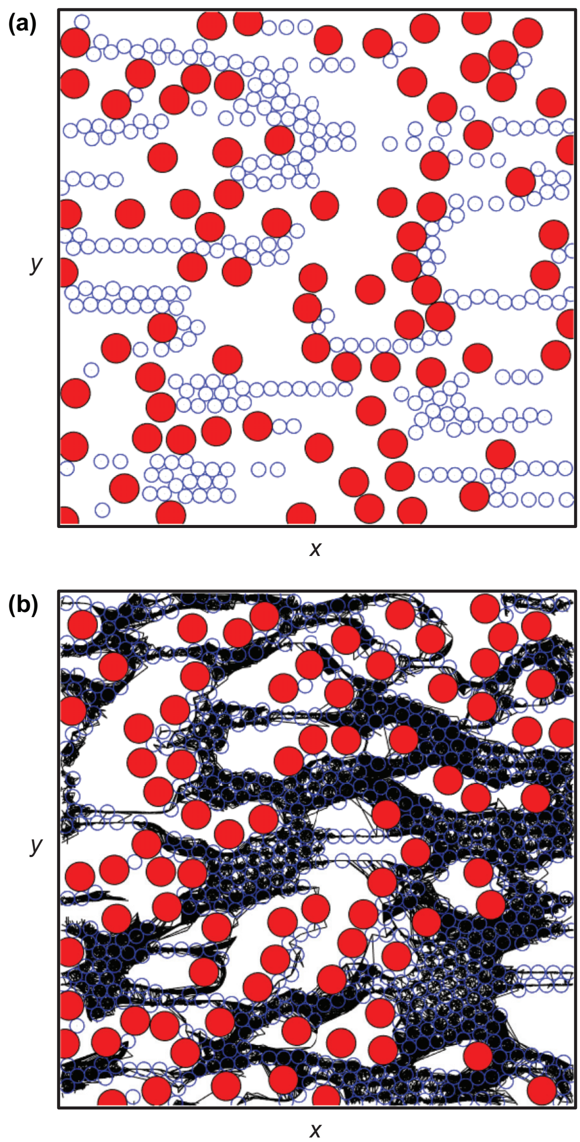

FIG. 1. Obstacle locations (red circles) and mobile disk locations (blue) along with trajectory lines indicating the net translation of the mobile disks from one cycle to the next over a time of $N_c = 100$ driving cycles. The disk positions are shown at the end of the drive cycle when the drive is about to switch from the $-x$ direction back to the $+x$ direction. (a) A completely reversible state at $A = 0.02$ and $\rho = 0.368$, where all of the disks return to the same position at the end of each driving cycle. The trajectory lines have zero length and thus do not appear in the panel. (b) An irreversible state at $A = 0.015$ and $\rho = 0.579$. The trajectory lines are finite and disordered.

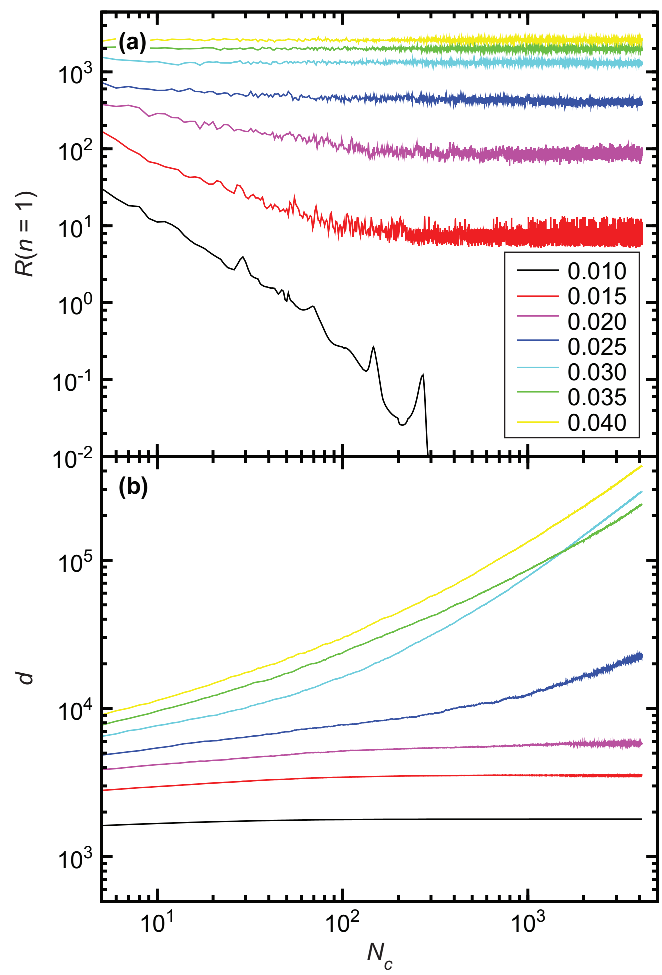

FIG. 2. A sample with total disk density $\rho = 0.398$ at varied drive amplitudes $A = 0.01$ to $A = 0.04$. (a) The distance $R(n = 1)$ traveled by the disks in a single driving cycle vs the total number of elapsed driving cycles N_c, where we have set $t_0 = N_c - 1$ in the calculation of R. (b) The total distance traveled d vs N_c. For $A = 0.01$, 0.015, and 0.02, the system reaches a reversible state. For $A = 0.025$, the system is irreversible but shows subdiffusive behavior, and for $A = 0.03$, 0.035, and 0.04, the motion is irreversible with regular diffusion.

direction. In Fig. 1 we plot the trajectories of the disks showing the motion from the end of one drive cycle to the end of the next drive cycle during $N_c = 100$ cycles, but in the reversible state of Fig. 1(a), these trajectories are of zero length and do not appear in the panel. Figure 1(b) shows an irreversible state at $A = 0.015$ and $\rho = 0.579$. Here, almost all of the disks participate in the irreversible behavior. The system still forms a heterogeneous state in which temporarily clogged and flowing regions coexist as a function of time, but the arrangement and location of the clogged regions changes over time instead of reaching a permanent repeating cycle.

In Fig. 2(a), for a sample with $\rho = 0.398$ under different drive amplitudes A, we plot $R(n = 1)$, the distance the disks travel during a single cycle, as a function of the total number N_c of elapsed cycles. Here we set $t_0 = N_c - 1$ in the calculation of R. Figure 2(b) shows the corresponding total distance traveled d versus N_c. For $A = 0.01$, 0.015, and 0.02, the system reaches a reversible state in which d saturates to a constant value. When $A = 0.01$, in the steady state the system is reversible after one cycle, so $R(n = 1)$ drops to zero in Fig. 2(a), while for $A = 0.015$ and 0.02, the steady-state positions recur only after multiple cycles, so the $R(n = 1)$ curve saturates to a finite value. For $A = 0.025$ the system is irreversible, but during an extended period of time d grows less than linearly with time, indicating subdiffusive behavior.

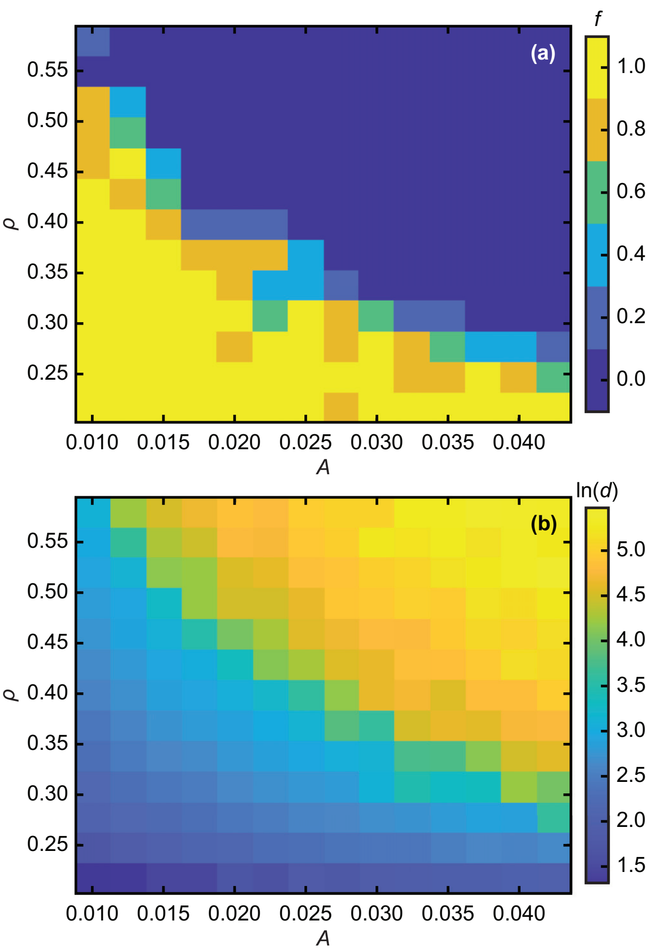

FIG. 3. (a) Heat map of the fraction f of the five different disorder realizations that reached reversible states plotted as a function of ρ vs A. (b) Heat map of $\ln[d(N_c = 3000)]$, the total displacement measured during $N_c = 3000$ driving cycles with $t_0 = 1000$ driving cycles, as a function of ρ vs A.

In the irreversible states at $A = 0.03$, 0.035, and 0.04, d grows linearly with time, a signature of Brownian diffusion.

In Fig. 3(a), we plot a heat map showing the fraction f of the five different disorder realizations that reached reversible states as a function of density ρ versus drive amplitude A. As ρ decreases, the threshold value of A at which irreversible behavior disappears shifts upward, so that reversible states appear for small ρ and A while irreversible states appear for large ρ and A. The boundary separating reversible and irreversible states is not sharp; instead, the disorder realizations are split with a portion of the realizations becoming reversible and the remaining realizations remaining irreversible. In our study, we focused on densities less than $\rho = 0.6$; however, for higher densities, the system could become completely clogged or mostly clogged, in which case the fraction of reversible states could increase again. In Fig. 3(b) we plot a heat map of the logarithm of $d(N_c = 3000)$, measured using $t_0 = 1000$ driving cycles, as a function of ρ versus A. Near the crossover from reversible to irreversible behavior, the total displacement begins to increase significantly.

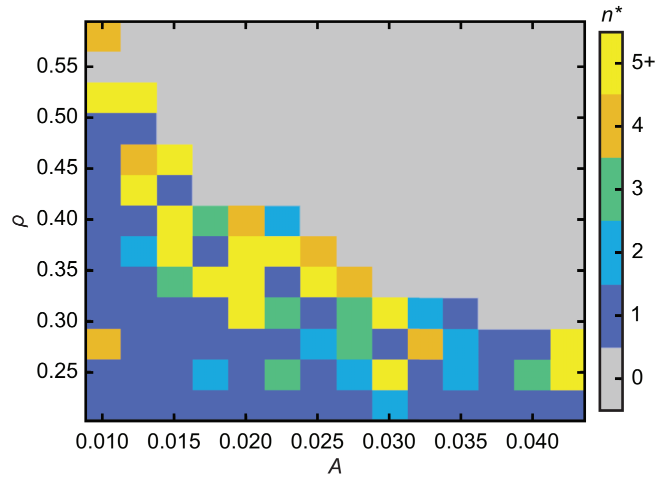

FIG. 4. Heat map of n^*, the smallest value of n for which $R(n)$ reaches zero in the reversible regime, as a function of ρ vs A. When $n^* > 1$, the state is multicycle reversible. In the irreversible regime, we mark $n^* = 0$. In the reversible regime, the value of n^* is averaged only over disorder realizations that were reversible.

By measuring $R(n)$ for different values of n in the reversible regime, we can determine how many drive cycles are required for the disks to reach their original positions. The smallest value of n for which $R(n)$ reaches zero in the reversible regime is labeled n^*. In Fig. 4, we plot a heat map of n^* as a function of ρ versus A. In the reversible regime, we average n^* only over the disorder realizations that were reversible, while in the irreversible regime where the measure is not defined, we mark $n^* = 0$. For low ρ and low A, we primarily find $n^* = 1$, meaning that most of the states are reversible after one cycle, while near the crossover from reversible to irreversible behavior, we find multicycle reversible states with $n^* = 5$ or more, and even observed one state that was reversible after $n^* = 24$ drive cycles.

In Fig. 5, we plot a heat map as a function of ρ versus A of the exponent α obtained from fits to $d \propto N_c^{\alpha}$. In a reversible

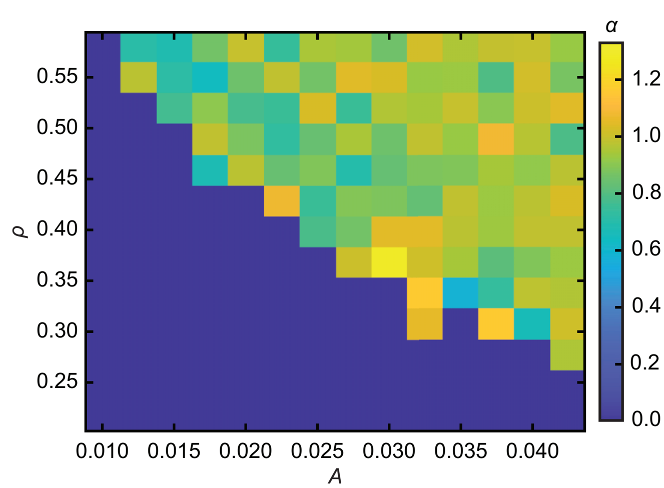

FIG. 5. Heat map as a function of ρ vs A of the exponent α obtained from a fit to $d \propto N_c^{\alpha}$. $\alpha = 0$ indicates reversible behavior, and $\alpha = 1.0$ indicates diffusive behavior.

state, $\alpha = 0$, while a value of $\alpha = 1.0$ indicates Brownian motion. We find regions in which $0 < \alpha < 1$, indicating that subdiffusion is occurring over an extended number of drive cycles. In these instances, the system forms what we call an intermediate irreversible state where large sections of the system act reversibly, but there are localized regions in which chaotic motion occurs. These localized regions can slowly move through the sample after many cycles. Such intermediate reversible states, where there are localized regions of irreversible behavior that coexist with reversible regions, are likely produced by a screening effect from the obstacles, which prevents irreversible regions from making contact with spatially separated reversible regions of the sample. In the irreversible regime of sheared systems without obstacles, no such screening exists and the irreversible motion can spread unhindered throughout the sample.

There is significant scatter in the values of the exponent α in Fig. 5. It might be expected that the highest values of α, corresponding to the greatest amount of irreversible-induced diffusion, should appear for the highest values of ρ and A. This type of behavior has been observed in a sheared system of dilute colloids as the shear amplitude is increased; however, going to high particle densities in the presence of obstacles as we do here can significantly change the behavior at high amplitude compared with the dilute case. The obstacles provide locations where localized jammed or clogged states can appear. Having jammed or clogged regions present in the sample, even if it is during only a portion of the driving cycle, can reduce the effective irreversible diffusion of the particles and lower the value of α as ρ or A increase, rather than giving larger values of α as would be expected in a dilute system.

We have also found states that show local irreversibility but do not exhibit long-time diffusion, again due to a screening effect of the obstacles. For example, if obstacles completely surround a region of disks, this region can undergo irreversible or chaotic motion that is effectively trapped and cannot interact with other parts of the system. These disks can continuously change their configurations, so their behavior is irreversible, but the confinement effect limits the maximum distance they can travel and bounds the maximum possible diffusion. In this way, a portion of the system would be locally ergodic, but the overall system is not globally ergodic. If the confined region is sufficiently small, the disks may be able to regain their original positions eventually, but they will not repeatedly return to these original positions in a periodic manner, so they will never enter a multicycle reversible state. Figure 6 shows an example of this behavior at $A = 0.01$ and $\rho = 0.519$, where there is no long-time diffusion, but there are two regions that are locally chaotic.

In our work, we consider five disorder realizations per parameter set in order to obtain a general outline of the different behaviors. A more careful study is needed to examine how fluctuations or other quantities would scale near the boundaries between the different behavior regimes. Several features complicate such a study compared with systems without quenched disorder. If there are no obstacles, below the transition to irreversibility the system can enter a reversible state and eventually organize to a collisionless state. For systems with quenched disorder, certain regions of the sample may effectively be cut off from other regions of the sample.

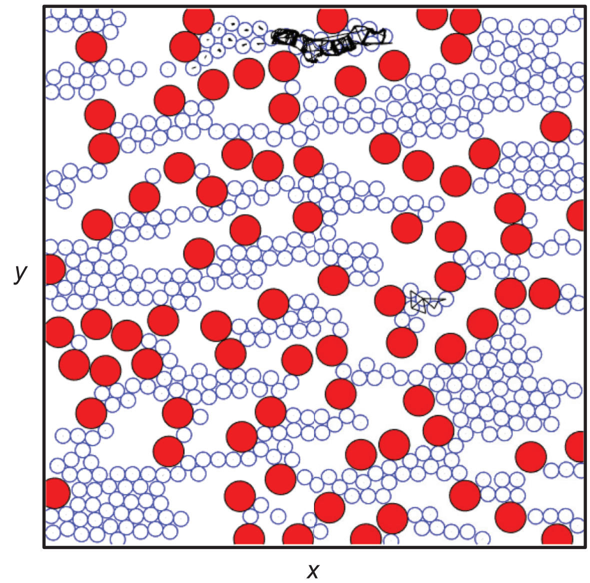

FIG. 6. Obstacle locations (red circles) and mobile disk locations (blue) along with trajectory lines indicating the net translation of the mobile disks from one cycle to the next over a time of $N_c = 100$ driving cycles in a state with two local regions of irreversible behavior but no long time diffusion at $\rho = 0.519$ and $A = 0.01$.

As a result, a portion of the disks may not have enough available space to reach collisionless or reversible states, so specific disorder realizations might produce entirely reversible states or regions of irreversibility. This issue does not arise when quenched disorder is not present. A future direction for study would be to consider a fixed density and carefully tune the amplitude through the transition to irreversibility for a large ensemble of disorder realizations, making it possible to quantify how the fraction of irreversible realizations varies as the transition is approached from either side.

IV. MULTICYCLE COMBINATORIAL REVERSIBLE STATES

In previous work in dense amorphous systems, multicycle reversible states were observed in which the particles form complex loop-like orbits that return to the same point after $N = n^*$ cycles [26,32–34]. In these systems, the particle orbits are different during each of the N driving cycles and only repeat once the entire cycle has been completed. Additionally, multicycle states are linked to the occurrence of distinct plastic events that can interact with each other through a long-range strain field. In our system, the reversible multicycle state is associated with groups of particles which can adopt the same macroscopic configuration multiple times during the full cycle, but which only reach the original microscopic disk configuration after the cycle is complete, creating what we call a combinatorial reversible state.

In Fig. 7, we show an example of a combinatorial reversible state where we highlight the positions of 14 disks and three obstacles in a small portion of a sample with $\rho = 0.337$ and $A = 0.025$ that is multicycle reversible. The white disks return to their original positions after every cycle, and we give distinct colors to the nine disks that reach different positions

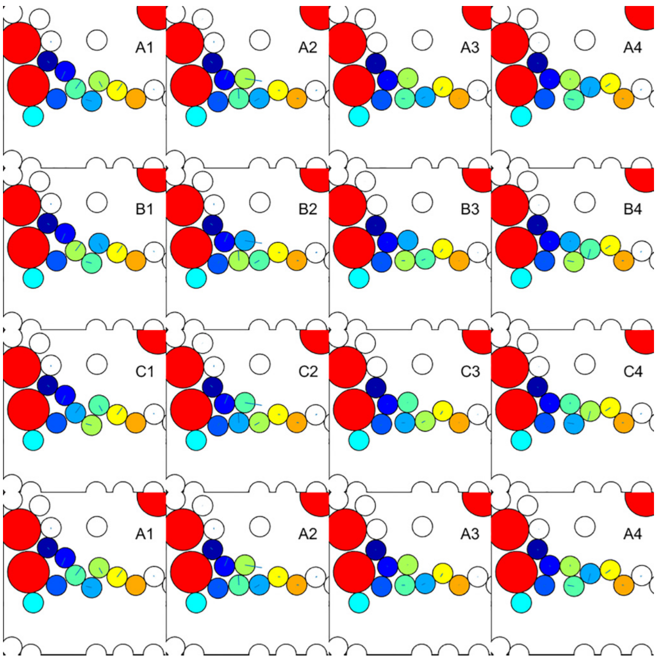

FIG. 7. Illustration of a combinatorial reversible state at $\rho = 0.337$ and $A = 0.025$ where the obstacle locations (large red circles), nonexchanging mobile disks (white circles), and exchanging mobile disks (small colored circles) are shown in only a small portion of the sample. The small trajectory lines indicate the net distance moved by each disk compared with its position at the end of the previous driving cycle. The disks return to their original positions every twelve cycles. Each panel shows the disk configuration at the end of a drive cycle. Time increases from left to right and top to bottom so that the cycle sequence is A1-A2-A3-A4-B1-B2-B3-B4-C1-C2-C3-C4. The macroscopic disk configurations repeat every four drive cycles, so that A1, B1, and C1 have the same macroscopic disk configuration, but the individual disks are permuted within this configuration.

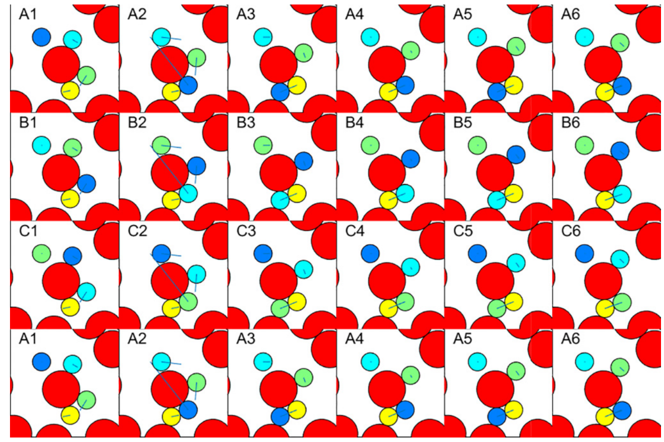

FIG. 8. Illustration of a different small region of the combinatorial reversible state from Fig. 7 at $\rho = 0.337$ and $A = 0.025$, showing the obstacle locations (large red circles) and exchanging mobile disks (small colored circles). The small trajectory lines indicate the net distance moved by each disk compared with its position at the end of the previous driving cycle. The disks return to their original positions every 18 cycles. Each panel shows the disk configuration at the end of a drive cycle. Time increases from left to right and top to bottom. The macroscopic disk configurations repeat every six drive cycles, so that A1, B1, and C1 have the same macroscopic disk configuration, but the individual disks are permuted within this configuration.

from cycle to cycle but only return to their original positions after twelve cycles. The trajectory lines connect the starting point of the disk from the end of the previous drive cycle to its ending point at the end of the illustrated drive cycle.

It is important to remember that in between the snapshots shown in each panel of Fig. 7, the disks move back and forth through a complete driving cycle, so that although their net motion is small, their actual motion is not small. Panel A1 shows the starting configuration. The sample progresses through configurations A2, A3, and A4, and after a total of four drive cycles, the macroscopic disk configuration in panel B1 is exactly the same as that of panel A1. The individual disk positions are not the same, however; the blue, green, and blue-green disks at the center of the image have exchanged places. After four more cycles, the system has passed through states B2, B3, and B4, and reached configuration C1. This is again macroscopically the same as A1 but microscopically different, with the blue, green, and blue-green disks having rotated into yet another arrangement. Four cycles later, the system passes through C2, C3, and C4, and reaches the original state A1. Similar combinatoric swaps separate the macroscopically identical but microscopically distinct states A2, B2, and C2. The same is true for states A3, B3, and C3 as well as states A4, B4, and C4. In this way, the disks are fully reversible after 12 cycles, but their macroscopic configuration is reversible every four cycles. This particular region of the sample acts like a small rotating gear.

In Fig. 8, we illustrate a different small portion of the sample from Fig. 7. Here the disks return to their original positions every 18 drive cycles but the macroscopic disk configuration repeats every six drive cycles. The lines highlight the net motion of the particles from their locations at the end of the previous driving cycle. To understand the motion of the disks, it is even more important to keep in mind the fact that the disks translate through an entire drive cycle in between consecutive frames of the figure. As a result, rather than the relatively simple rotation illustrated in Fig. 7, we find in Fig. 8 that the disks can do a leapfrog position exchange. The initial configuration is labeled A1. After one drive cycle, in A2, the dark blue disk has interposed itself between the green and yellow disks. Small adjustments of the disk positions occur during cycles A3, A4, A5, and A6, until on the sixth cycle, in B1, the macroscopic disk configurations of A1 are reproduced but with a permutation in the disk positions. The same pattern repeats, with the light blue disk interposing itself between the yellow and dark blue disks in panel B2, followed by small disk adjustments for four cycles and a return to the A1 macroscopic configuration in the twelfth cycle, C1. After 18 cycles the original disk configuration is restored. The leapfrog exchange does not occur while the disks are surrounding the pictured obstacle; instead, it is as the disks move during the driving cycle and make contact with other obstacles (out of frame) and disks that their positions are swapped. The localized nature of the multicycle reversible states illustrated in Figs. 7 and 8 makes it possible for a single system to have numerous multicycle states present simultaneously, so that the entire system becomes fully reversible only after all of the multicycle states have reached their starting configurations at the same time. In the case of the combination shown, a 12-cycle reversible state with an 18-cycle reversible state, full reversibility happens only after 36 cycles. The number of possible multicycle regions increases as the boundary between the reversible and irreversible behavior is approached, and the necessity for simultaneous synchronization of multiple reversible regions is responsible for the large values of n^* found near the reversible-irreversible boundary in Fig. 4.

At low ρ, it might be expected that the system would always reach a reversible state except for large driving amplitudes, as found in the periodically sheared low density colloidal system. In systems without quenched disorder at low densities, each particle has ample space to organize into an arrangement where particle-particle collisions no longer occur. In our system, the obstacle positions are fixed so the obstacles are unable to move out of the way to prevent disk-obstacle collisions. If the density of obstacles is sufficiently high, such disk-obstacle collisions become unavoidable, and at best the disks can organize themselves to prevent disk-disk collisions from occurring. The fixed obstacles limit the amount of space available for this rearrangement, making disk-disk collisions more likely since the disks are being forced into a smaller total area. We find that the low density states contain a combination of disks that never undergo collisions and have reversible motion, disks that collide only with obstacles but are still reversible, and, crucially, disks that continue to collide with each other and with obstacles but still reach a reversible state. The latter set of disks do not return to the same state after each cycle but instead undergo a permutation or effective rotation that causes the original state to reappear only after multiple drive cycles have elapsed. Hence, the reversible states we illustrate in Figs. 7 and 8 are distinct from the random organization states since collisions are never eliminated but continue to occur permanently.

V. DISCUSSION

In this work, we have introduced our reversible-irreversible system of disks cyclically driven past obstacles, but there are many future directions to consider. For example, for a given disorder realization, it would be interesting to measure whether an initially irreversible portion of the sample grows in extent as the system is pushed deeper into the irreversible regime, or whether the irreversible patch remains roughly the same size and instead the number of irreversible patches increases. In the latter case, the irreversible patches might merge through a percolative process. We considered monodisperse mobile disks, but it would also be possible to introduce bidisperse mobile disk sizes, where one species is much larger than the other. Here, it could be possible to reach a state where one species is jammed or reversible and the other species remains mobile and irreversible. We concentrated on the reversible-irreversible transition for low and intermediate densities; however, at higher densities, there could be a transition from reversible-irreversible behavior to jamming or the formation of a rigid solid that moves elastically back and forth over some distance. If this were the case, there could be a second irreversible to reversible transition that occurs at high densities. It would also be interesting to explore the effect of making the particles flexible, adding rotational degrees of freedom, or introducing thermal fluctuations.

VI. SUMMARY

We have examined the crossover from reversible to irreversible behavior in a system of disks moving through a random obstacle array under cyclic drive. We measure the net displacement of the disks after n cycles for different disk densities and drive amplitudes. For high densities and high amplitudes, we find an irreversible state in which the disks undergo diffusive motion. In the reversible state, for low densities and low amplitudes the system returns to its original configuration after every drive cycle, but as the reversible-irreversible boundary is approached, multicycle reversible states appear in which the disks return to their original configurations after two or more driving cycles. We also observe multicycle combinatorial reversible states in which the macroscopic disk configurations repeat after a subset of cycles but the individual disk positions have been permuted, so that the original positions are restored only after a sufficient number of permutation cycles occur. This can produce very large multicycle reversibility when more than one multicycle combinatorial region is present in the sample and the regions do not have the same reversible period. We find that some irreversible states have what we call intermediate irreversible properties, where regions of disks exhibit chaotic irreversible behavior that remains localized for long times due to a screening effect from the obstacles. In the intermediate state, these irreversible regions gradually move around the system. In other cases, the localized irreversible regions become completely trapped, so there is no long time diffusion in the system even though the behavior remains irreversible. Our results show that disks driven through obstacles have behaviors similar to what is found for dilute sheared systems, where reversible orbits form when no collisions occur between the particles, as well as behaviors similar to what is observed in sheared dense amorphous systems, where interactions between reversible regions can produce multicycle reversibility.

ACKNOWLEDGMENTS

This research was supported in part by the Notre Dame Center for Research Computing. Work at the University of Notre Dame (D.M., M.R.E.) was supported by the U.S. Department of Energy, Office of Basic Energy Sciences, under Award No. DE-SC0005051. We gratefully acknowledge the support of the U.S. Department of Energy through the LANL/LDRD program for this work. The work at LANL was supported by the U.S. Department of Energy through the Los Alamos National Laboratory. Los Alamos National Laboratory is operated by Triad National Security, LLC, for the National Nuclear Security Administration of the U.S. Department of Energy (Contract No. 892333218NCA000001).

[1] S. Bhattacharya and M. J. Higgins, Dynamics of a disordered flux line lattice, Phys. Rev. Lett. **70**, 2617 (1993).

[2] C. Reichhardt and C. J. O. Reichhardt, Depinning and nonequilibrium dynamic phases of particle assemblies driven over random and ordered substrates: A review, Rep. Prog. Phys. **80**, 026501 (2017).

[3] A. Pertsinidis and X. S. Ling, Statics and dynamics of 2D colloidal crystals in a random pinning potential, Phys. Rev. Lett. **100**, 028303 (2008).

[4] W. Jiang, X. Zhang, G. Yu, W. Zhang, X. Wang, M. B. Jungfleisch, J. E. Pearson, X. Cheng, O. Heinonen, K. L. Wang, Y. Zhou, A. Hoffmann, and S. G. E. te Velthuis, Direct observation of the skyrmion Hall effect, Nat. Phys. **13**, 162 (2017).

[5] C. Reichhardt, C. J. O. Reichhardt, and M. V. Milošević, Statics and dynamics of skyrmions interacting with disorder and nanostructures, Rev. Mod. Phys. **94**, 035005 (2022).

[6] M. Le Blay, M. Adda-Bedia, and D. Bartolo, Emergence of scale-free smectic rivers and critical depinning in emulsions driven through disorder, Proc. Natl. Acad. Sci. USA **117**, 13914 (2020).

[7] A. Morin, N. Desreumaux, J.-B. Caussin, and D. Bartolo, Distortion and destruction of colloidal flocks in disordered environments, Nat. Phys. **13**, 63 (2017).

[8] C. Sándor, A. Libál, C. Reichhardt, and C. J. O. Reichhardt, Dynamic phases of active matter systems with quenched disorder, Phys. Rev. E **95**, 032606 (2017).

[9] C. J. Olson Reichhardt, E. Groopman, Z. Nussinov, and C. Reichhardt, Jamming in systems with quenched disorder, Phys. Rev. E **86**, 061301 (2012).

[10] I. Zuriguel, D. R. Parisi, R. C. Hidalgo, C. Lozano, A. Janda, P. A. Gago, J. P. Peralta, L. M. Ferrer, L. A. Pugnaloni, E. Clément, D. Maza, I. Pagonabarraga, and A. Garcimartín, Clogging transition of many-particle systems flowing through bottlenecks, Sci. Rep. **4**, 7324 (2015).

[11] H. T. Nguyen, C. Reichhardt, and C. J. O. Reichhardt, Clogging and jamming transitions in periodic obstacle arrays, Phys. Rev. E **95**, 030902(R) (2017).

[12] G. Gerber, S. Rodts, P. Aimedieu, P. Faure, and P. Coussot, Particle-size-exclusion clogging regimes in porous media, Phys. Rev. Lett. **120**, 148001 (2018).

[13] R. L. Stoop and P. Tierno, Clogging and jamming of colloidal monolayers driven across disordered landscapes, Commun. Phys. **1**, 68 (2018).

[14] C. Reichhardt, I. Regev, K. Dahmen, S. Okuma, and C. J. O. Reichhardt, Reversible to irreversible transitions in periodic driven many-body systems and future directions for classical and quantum systems, Phys. Rev. Res. **5**, 021001 (2023).

[15] D. J. Pine, J. P. Gollub, J. F. Brady, and A. M. Leshansky, Chaos and threshold for irreversibility in sheared suspensions, Nature (London) **438**, 997 (2005).

[16] L. Corte, P. M. Chaikin, J. P. Gollub, and D. J. Pine, Random organization in periodically driven systems, Nat. Phys. **4**, 420 (2008).

[17] D. Hexner and D. Levine, Hyperuniformity of critical absorbing states, Phys. Rev. Lett. **114**, 110602 (2015).

[18] E. Tjhung and L. Berthier, Hyperuniform density fluctuations and diverging dynamic correlations in periodically driven colloidal suspensions, Phys. Rev. Lett. **114**, 148301 (2015).

[19] J. H. Weijs, R. Jeanneret, R. Dreyfus, and D. Bartolo, Emergent hyperuniformity in periodically driven emulsions, Phys. Rev. Lett. **115**, 108301 (2015).

[20] C. Reichhardt and C. J. O. Reichhardt, Reversibility, pattern formation, and edge transport in active chiral and passive disk mixtures, J. Chem. Phys. **150**, 064905 (2019).

[21] Q.-L. Lei and R. Ni, Hydrodynamics of random-organizing hyperuniform fluids, Proc. Natl. Acad. Sci. USA **116**, 22983 (2019).

[22] J. D. Paulsen, N. C. Keim, and S. R. Nagel, Multiple transient memories in experiments on sheared non-Brownian suspensions, Phys. Rev. Lett. **113**, 068301 (2014).

[23] N. C. Keim, J. D. Paulsen, Z. Zeravcic, S. Sastry, and S. R. Nagel, Memory formation in matter, Rev. Mod. Phys. **91**, 035002 (2019).

[24] C. F. Schreck, R. S. Hoy, M. D. Shattuck, and C. S. O'Hern, Particle-scale reversibility in athermal particulate media below jamming, Phys. Rev. E **88**, 052205 (2013).

[25] J. R. Royer and P. M. Chaikin, Precisely cyclic sand: Self-organization of periodically sheared frictional grains, Proc. Natl. Acad. Sci. USA **112**, 49 (2015).

[26] I. Regev, T. Lookman, and C. Reichhardt, Onset of irreversibility and chaos in amorphous solids under periodic shear, Phys. Rev. E **88**, 062401 (2013).

[27] D. Fiocco, G. Foffi, and S. Sastry, Oscillatory athermal quasistatic deformation of a model glass, Phys. Rev. E **88**, 020301(R) (2013).

[28] D. Fiocco, G. Foffi, and S. Sastry, Encoding of memory in sheared amorphous solids, Phys. Rev. Lett. **112**, 025702 (2014).

[29] N. C. Keim and P. E. Arratia, Mechanical and microscopic properties of the reversible plastic regime in a 2D jammed material, Phys. Rev. Lett. **112**, 028302 (2014).

[30] N. V. Priezjev, Reversible plastic events during oscillatory deformation of amorphous solids, Phys. Rev. E **93**, 013001 (2016).

[31] N. V. Priezjev, Collective nonaffine displacements in amorphous materials during large-amplitude oscillatory shear, Phys. Rev. E **95**, 023002 (2017).

[32] M. O. Lavrentovich, A. J. Liu, and S. R. Nagel, Period proliferation in periodic states in cyclically sheared jammed solids, Phys. Rev. E **96**, 020101(R) (2017).

[33] K. Khirallah, B. Tyukodi, D. Vandembroucq, and C. E. Maloney, Yielding in an integer automaton model for amorphous solids under cyclic shear, Phys. Rev. Lett. **126**, 218005 (2021).

[34] N. C. Keim and J. D. Paulsen, Multiperiodic orbits from interacting soft spots in cyclically sheared amorphous solids, Sci. Adv. **7**, eabg7685 (2021).

[35] N. Mangan, C. Reichhardt, and C. J. O. Reichhardt, Reversible to irreversible flow transition in periodically driven vortices, Phys. Rev. Lett. **100**, 187002 (2008).

[36] S. Okuma, Y. Tsugawa, and A. Motohashi, Transition from reversible to irreversible flow: Absorbing and depinning transitions in a sheared-vortex system, Phys. Rev. B **83**, 012503 (2011).

[37] G. Pasquini, M. M. Bermúdez, and V. Bekeris, AC dynamic reorganization and critical phase transitions in superconducting vortex matter, Supercond. Sci. Technol. **34**, 013003 (2021).

[38] S. Maegochi, K. Ienaga, S. Kaneko, and S. Okuma, Critical behavior near the reversible-irreversible transition in periodically

driven vortices under random local shear, Sci. Rep. **9**, 16447 (2019).

[39] S. Maegochi, K. Ienaga, and S. Okuma, Critical behavior of density-driven and shear-driven reversible-irreversible transitions in cyclically sheared vortices, Sci. Rep. **11**, 19280 (2021).

[40] K. Litzius, I. Lemesh, B. Krüger, P. Bassirian, L. Caretta, K. Richter, F. Büttner, K. Sato, O. A. Tretiakov, J. Förster, R. M. Reeve, M. Weigand, I. Bykova, H. Stoll, G. Schütz, G. S. D. Beach, and M. Kläui, Skyrmion Hall effect revealed by direct time-resolved X-ray microscopy, Nat. Phys. **13**, 170 (2017).

[41] B. L. Brown, U. C. Täuber, and M. Pleimling, Effect of the Magnus force on skyrmion relaxation dynamics, Phys. Rev. B **97**, 020405(R) (2018).

[42] C. Reichhardt and C. J. O. Reichhardt, Reversible to irreversible transitions for cyclically driven particles on periodic obstacle arrays, J. Chem. Phys. **156**, 124901 (2022).